Available online at www.sciencedirect.com
SCIENCE DIRECT®
Catalysis Today 93–95 (2004) 155–161
CATALYSIS TODAY
www.elsevier.com/locate/cattod

SBA-15-supported iron phosphate catalyst for partial oxidation of methane to formaldehyde

Ye Wang*, Xiaoxing Wang, Zheng Su, Qian Guo, Qinghu Tang, Qinghong Zhang, Huilin Wan

State Key Laboratory of Physical Chemistry of Solid Surfaces, Department of Chemistry, Xiamen University, Xiamen 361005, PR China

Abstract

SBA-15-supported iron phosphate ($FePO_4$) has been characterized with XRD, TEM, Raman spectroscopy and H_2-TPR, and studied for the partial oxidation of CH_4 with O_2. The characterizations suggest that the $FePO_4$ species with loading amount lower than 40 wt.% are encapsulated within the mesoporous channels of SBA-15, and these species possibly exist as small $FePO_4$ clusters with the local coordination environment of iron being similar to that in the crystalline $FePO_4$. However, these encapsulated $FePO_4$ clusters could be reduced at remarkably lower temperatures than the crystalline $FePO_4$. The SBA-15-supported $FePO_4$ catalysts exhibit higher CH_4 conversion and HCHO selectivity than the unsupported and the MCM-41-supported ones in the partial oxidation of CH_4 with O_2. The catalyst with a loading amount of 5 wt.% shows the highest HCHO selectivity at a given CH_4 conversion and the highest HCHO formation rate based on the amount of $FePO_4$ in the catalyst. It is likely that the improved catalytic performances of the SBA-15-supported samples are related to the enhanced redox properties of $FePO_4$ species, the large porous diameter and the high inertness of SBA-15.

Keywords: Methane; Partial oxidation; Formaldehyde; Iron phosphate; SBA-15

1. Introduction

Partial oxidation of CH_4 to useful oxygenates such as CH_3OH and HCHO remains as a great challenge in the new century. Many studies have been contributed to this field but the current state-of-the-art is still far from commercial consideration [1–5]. Wang and Otsuka reported that an iron phosphate ($FePO_4$) catalyst exhibited high selectivity to useful oxygenates during the partial oxidation of CH_4 or C_2H_6 with O_2–H_2 or N_2O [6]. Formaldehyde could also be selectively formed during the partial oxidation of CH_4 with O_2 alone over the $FePO_4$ catalyst. McCormick and co-workers found that the supporting of $FePO_4$ onto silica enhanced the conversion of CH_4 to HCHO [7].

Since mesoporous molecular sieves possess well-ordered mesoporous channels and large surface areas, the active component may thus be tailored in their nano-order spaces. Recently, we have reported that the supporting of $FePO_4$ onto MCM-41 with loading amount of 20–40 wt.% increases both CH_4 conversion and HCHO selectivity in the partial oxidation of CH_4 [8]. SBA-15, which possesses larger pores, thicker walls and higher thermal stability as compared with other mesoporous silicas [9] may be used as a promising catalyst support, particularly for reactions occurring at high temperatures. Furthermore, because of the larger porous diameter (5–30 nm) of SBA-15 the partial oxidation product would facilely leave the catalyst, decreasing the probability of its consecutive oxidation to deep oxidation products. SBA-15-supported vanadium oxide has been reported to be more effective for the oxidative dehydrogenation of C_3H_8 [10] and the photo-assisted oxidation of CH_4 at low temperatures [11] than the MCM-41- and silica-supported catalysts. We have recently communicated that vanadium oxide and phosphorus-modified molybdenum oxide clusters encapsulated inside SBA-15 both show very high HCHO formation yield in the partial oxidation of CH_4 [12,13]. As a continuation of these researches, in the present study, the structural and catalytic properties of the $FePO_4$ introduced into SBA-15 for the partial oxidation of CH_4 with O_2 are investigated and compared with those of the unsupported and the MCM-41-supported $FePO_4$ catalysts.

2. Experimental

$FePO_4$ was prepared using the procedure described previously [6]. SBA-15 was synthesized with a procedure

* Corresponding author. Fax: +86 592 2183047.
E-mail address: yewang@jingxian.xmu.edu.cn (Y. Wang).

0920-5861/$ – see front matter © 2004 Elsevier B.V. All rights reserved.
doi:10.1016/j.cattod.2004.06.037

described elsewhere [9,13]. Typically, a homogeneous mixture composed of Pluronic P123 triblock copolymers (EO_{20}-PO_{70}-EO_{20}) and tetraethyl orthosilicate (TEOS) in hydrochloric acid was stirred at 308 K for 24 h and further treated at 370 K for 24 h. The resultant solid was filtered, washed, dried and finally calcined at 823 K for 6 h. $FePO_4$ was introduced into SBA-15 by an impregnation method. SBA-15 was immersed into the mixed solution of $Fe(NO_3)_3$ and $NH_4H_2PO_4$ (Fe/P = 1) and was allowed to stir for 12 h at room temperature. The slurry was then dried with continuous stirring. The dried powder was finally calcined at 823 K for 6 h. For comparison, MCM-41-supported $FePO_4$ has been prepared with a similar procedure as described elsewhere [8].

The catalysts were characterized by XRD, N_2-adsorption, TEM, UV- and Vis-Raman spectroscopy and H_2-TPR. XRD was performed with a Rigaku-D/Max-C X-ray diffractometer with Cu Kα radiation. N_2-adsorption at 77 K was carried out with a TriStar 3000 Surface area and Porosimetry analyser (Micromeritics). TEM was taken on a FEI Tecnai 30 electron microscope (Phillips Analytical) operated at an acceleration voltage of 300 kV. Raman spectroscopic measurements were carried out with a Renishaw UV–vis Raman System 1000R. The UV line at 325 nm from a Kimmon IK3201R-F He–Cd laser was used as the exciting source for UV Raman measurements. H_2-TPR was performed using a flow system equipped with a thermal conductivity detector. Temperature was increased at a rate of 10 K min^{-1} in a H_2–Ar (5% H_2) mixture after the pre-treatment in N_2 and O_2 followed by purge with highly pure N_2 at 823 K and cooling to 303 K. Typically, 100 mg of sample was used for each experiment.

The partial oxidation of CH_4 was carried out using a fixed-bed reactor (U-type quartz tube with inner diameter of 4 mm) operated at atmospheric pressure. The products were analysed by on-line gas chromatography. All the lines and valves between the exit of the reactor and the gas chromatographs were heated to 393 K to prevent the condensation of products. The typical reaction conditions were as follows: $W = 0.2$ g for supported samples and 0.5 g for $FePO_4$, $F = 60\ cm^3\ min^{-1}$, $P(CH_4) = 33.8$ kPa, $P(O_2) = 16.9$ kPa, $T = 673$–873 K. The details for the calculations of CH_4 conversion and product selectivities were shown elsewhere [8].

3. Results and discussion

3.1. Characterizations of SBA-15-supported iron phosphate

Fig. 1 shows the XRD patterns for the SBA-15-supported $FePO_4$ samples with different loading amount of $FePO_4$. The diffraction peaks at 2θ values of ca. 1.1°, 1.7° and 2.0° ascribed to the hexagonal regularity of porous structure of SBA-15 were sustained after the introduction of $FePO_4$ into SBA-15 up to 20 wt.% (Fig. 1A). These peaks became unobservable with further increases in the loading amount, indicating the de-organization at long range of the mesoporous structure. Although the collapse of mesoporous channels could be a reason, we think that the incorporation of $FePO_4$ species into the mesopores may also causes the irregularity at long range. The XRD patterns at high diffraction angles (Fig. 1B) showed that any crystalline phase of $FePO_4$ did not appear when the loading amount of $FePO_4$ was lower than 40 wt.%. Weak diffraction lines at 20.5° and 22° assignable to the tridymite-like phase of $FePO_4$ became observable for the sample with loading amount of 60 wt.%, while the unsupported $FePO_4$ was composed of mainly quartz-like phase

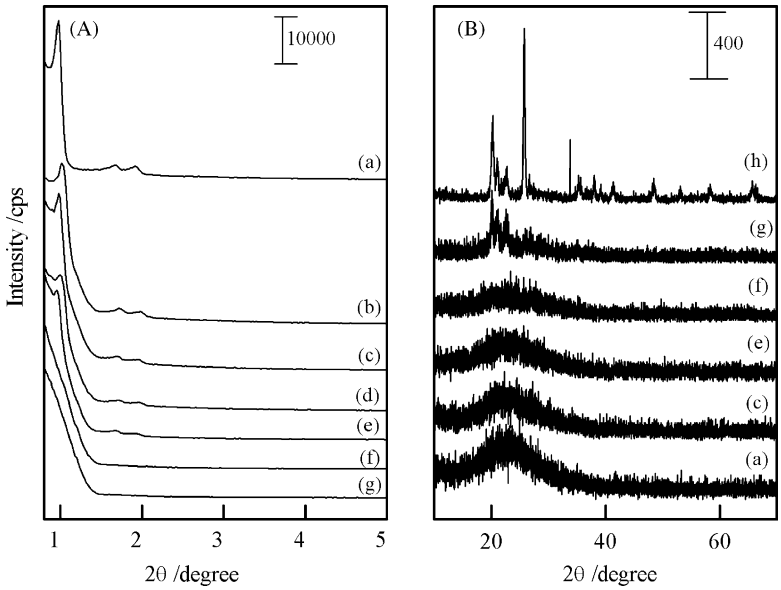

Fig. 1. XRD patterns at low and high diffraction angles: (a) SBA-15, (b) 5 wt.% $FePO_4$/SBA-15, (c) 10 wt.% $FePO_4$/SBA-15, (d) 15 wt.% $FePO_4$/SBA-15, (e) 20 wt.% $FePO_4$/SBA-15, (f) 40 wt.% $FePO_4$/SBA-15, (g) 60 wt.% $FePO_4$/SBA-15 and (h) $FePO_4$.

Table 1
Porous properties of SBA-15-supported $FePO_4$ with different loading amounts

Sample	Surface area ($m^2\ g^{-1}$)	Pore volume ($cm^3\ g^{-1}$)	Pore diameter (nm)
SBA-15	825	0.85	5.4
10 wt.% $FePO_4$/SBA-15	501	0.75	5.3
20 wt.% $FePO_4$/SBA-15	444	0.68	5.4
40 wt.% $FePO_4$/SBA-15	184	0.35	5.4
60 wt.% $FePO_4$/SBA-15	161	0.22	2.8
$FePO_4$	3.0	–	–

as well as a small amount of tridymite-like one. These results resemble those obtained for the MCM-41-supported $FePO_4$ and suggest that the $FePO_4$ species with loading amount of lower than 40 wt.% are probably located inside the mesoporous channels of SBA-15, dispersing on the wall surface or forming small clusters which are hard to be detected by XRD.

TEM observations further support the encapsulation of $FePO_4$ species within the mesopores. As typical examples, TEM images of the 15 wt.% $FePO_4$/SBA-15 are shown in Fig. 2. The hexagonal array of mesoporous channels was clearly observed. Moreover, small clusters encapsulated inside the mesoporous channels could also be discerned when Fig. 2b and c were compared. No large particles located outside the mesopores were observed for the 15 wt.% $FePO_4$/SBA-15 (Fig. 2a and b). The pore diameter evaluated from Fig. 2 was ca. 5.5 nm, consistent with the result obtained from N_2-adsorption measurements as shown in Table 1. The table also shows that both the BET surface area and the pore volume decrease with an increase in the loading amount of $FePO_4$. Decreases in the surface area, pore volume and pore diameter were likewise observed after the introduction of $FePO_4$ into MCM-41 which possessed pore diameter of ca. 3 nm [8].

Fig. 3 shows the UV Raman spectra of the SBA-15-supported $FePO_4$ samples. The unsupported $FePO_4$ exhibited two intense bands at 1015 and 1059 cm^{-1}, arising from the alternatively connected tetrahedral PO_4 and FeO_4 groups. The two bands were still observable for the SBA-15-supported $FePO_4$ samples, but they became broad and overlapped. This indicates that the local structure of iron in the $FePO_4$ species inside the mesopores of SBA-15 is similar to that in bulk $FePO_4$, i.e., iron is in tetrahedral coordination and the FeO_4 tetrahedron is surrounded by four PO_4 tetrahedra. The broadening of Raman bands may be related to the small size of the $FePO_4$ clusters within the mesoporous channels.

Fig. 4 shows the H_2-TPR results. The unsupported $FePO_4$ (20 mg used in Fig. 4) exhibited one asymmetric reduction peak at 963 K. The peak position was not changed by varying the amount of $FePO_4$ used for TPR experiment. However, the reduction peak remarkably shifted to lower temperatures for the $FePO_4$ species encapsulated in SBA-15. The main reduction peak for the sample with loading amount of 5 wt.% was at 783 and 180 K lower than that observed for the unsupported $FePO_4$. The reduction peak was slightly shifted to higher temperatures with increasing the loading amount of $FePO_4$ to 40 wt.%, and the peak temperatures were 813, 815 and 819 K for the samples with loading amount of 10, 20 and 40 wt.%, respectively. As the loading amount reached 60 wt.%, the main peak shifted to 848 K and a shoulder peak at 913 K appeared distinctly. The peak at 913 K prob-

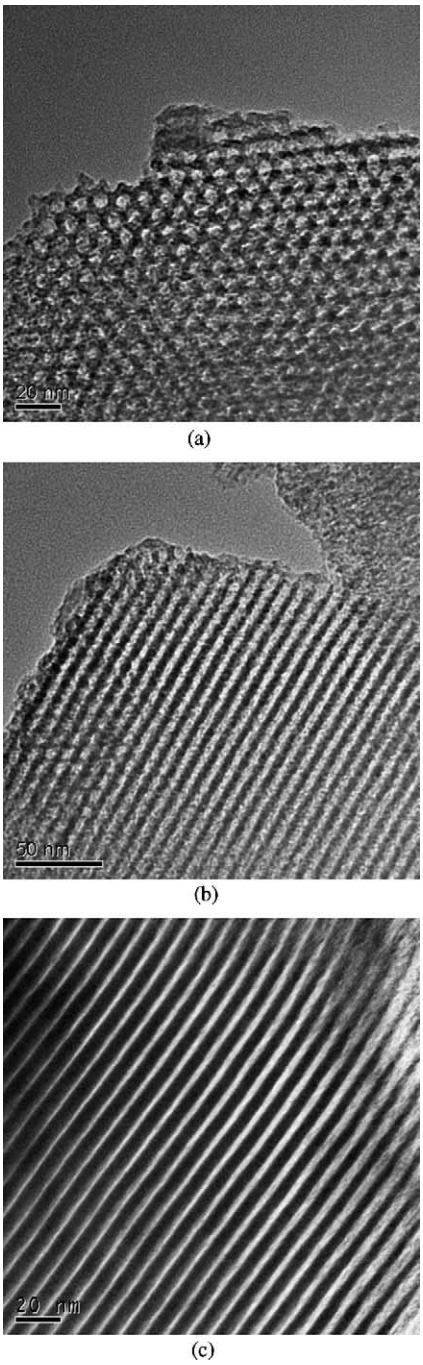

Fig. 2. TEM images of the 15 wt.% $FePO_4$/SBA-15 (a) and (b) and SBA-15 (c). (a) Taken with the beam parallel to the pore direction and (b) and (c) taken with the beam perpendicular to the pore direction.

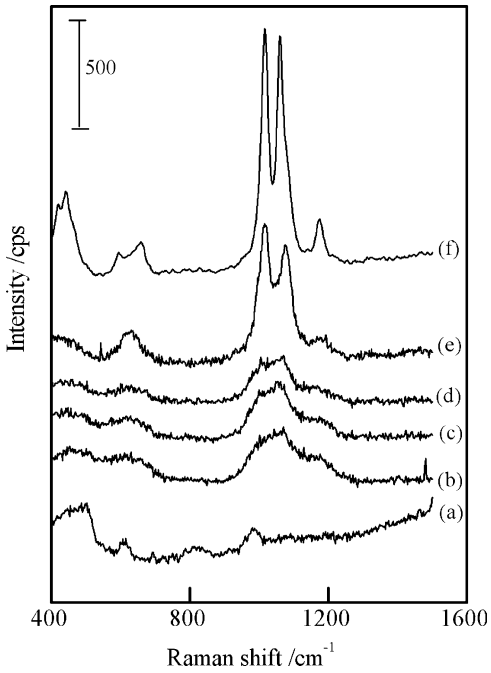

Fig. 3. Laser Raman spectra: (a) SBA-15, (b) 5 wt.% $FePO_4$/SBA-15, (c) 15 wt.% $FePO_4$/SBA-15, (d) 40 wt.% $FePO_4$/SBA-15, (e) 60 wt.% $FePO_4$/SBA-15 and (f) $FePO_4$.

ably arose from the reduction of the crystalline $FePO_4$ with tridymite-like structure as suggested by the XRD result in Fig. 1. With reference to our previous result that the reduction of the $FePO_4$ species within MCM-41 occurred at 796–813 K, the peak located at 783–848 K observed here

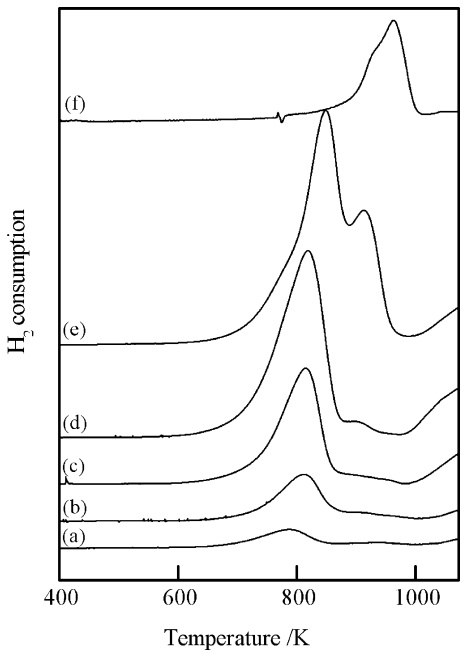

Fig. 4. H_2-TPR profiles: (a) 5 wt.% $FePO_4$/SBA-15, (b) 10 wt.% $FePO_4$/SBA-15, (c) 20 wt.% $FePO_4$/SBA-15, (d) 40 wt.% $FePO_4$/SBA-15, (e) 60 wt.% $FePO_4$/SBA-15 and (f) $FePO_4$.

was similarly ascribed to the reduction of the nano-sized $FePO_4$ species encapsulated within the mesoporous channels of SBA-15. These results strongly suggest that the small $FePO_4$ clusters encapsulated within the mesoporous channels of SBA-15 can be reduced at significantly lower temperatures as compared with the crystalline $FePO_4$.

3.2. Catalytic properties of SBA-15-supported iron phosphate

Table 2 shows the catalytic properties of SBA-15-supported $FePO_4$ samples with different loading amount. SBA-15 alone was almost inactive in the oxidation of CH_4 with O_2; CH_4 conversion was lower than 0.1% at 823 K. The bulk $FePO_4$ exhibited reasonably high CH_4 conversion and HCHO selectivity with O_2 as the oxidant as reported previously [6]. The supporting of $FePO_4$ to SBA-15 with loading amount of 5–40 wt.% increased both CH_4 conversion and HCHO selectivity although SBA-15 was almost inactive. HCHO yield varied only slightly with the loading amount changed from 5 to 20 wt.% at either 773 and 823 K. Since the activity of SBA-15 was negligible under the conditions in Table 2, the catalytic performance of the supported catalyst was due to the contribution of the encapsulated $FePO_4$ clusters. The rate of HCHO formation was thus evaluated based on the amount of $FePO_4$ species (per gram of $FePO_4$) existing in each catalyst. The comparison showed that the catalyst with the lowest loading amount (5 wt.%) of $FePO_4$ exhibited the best rate of HCHO formation based on the amount of $FePO_4$ species. It is thus likely that the higher dispersion of $FePO_4$ inside the mesoporous channels results in higher rate of HCHO formation.

It is known that HCHO selectivity generally decreases with an increase in CH_4 conversion because of the consecutive oxidation of HCHO into CO and CO_2. A better catalyst should have higher HCHO selectivity at the same CH_4 conversion level. Fig. 5 thus compares HCHO selectivity by changing CH_4 conversion with varying reaction temperature from 673 to 873 K over the SBA-15-supported and the unsupported catalysts. The result for the MCM-41-supported $FePO_4$ with a loading amount of 40 wt.% is also shown in the figure. This catalyst showed the highest HCHO selectivity at a given CH_4 conversion among the series of MCM-41-supported $FePO_4$ [8]. All the supported catalysts exhibited higher HCHO selectivity than the unsupported one at the same CH_4 conversion. Thus, the $FePO_4$ species encapsulated in the mesoporous channels possess noticeable advantages over the unsupported $FePO_4$ for the partial oxidation of CH_4 to HCHO. Detailed comparison showed that, at a given CH_4 conversion (>0.5%), the HCHO selectivity increased with the following sequence, $FePO_4$ < 40 wt.% $FePO_4$/MCM-41 < 40 wt.% $FePO_4$/SBA-15 < 20 wt.% $FePO_4$/SBA-15 < 15 wt.% $FePO_4$/SBA-15 < 10 wt.% $FePO_4$/SBA-15 < 5 wt.% $FePO_4$/SBA-15. In other words, among the SBA-15-supported $FePO_4$ series, the sample with the lowest loading amount (5 wt.%) was the

Table 2
SBA-15-supported iron phosphate catalysts for partial oxidation of methane using oxygen

Catalyst	Temperature (K)	CH_4 conversion (%)	HCHO selectivity (%)	HCHO yield (%)	Rate of HCHO formation (mmol h^{-1} (g-$FePO_4$)$^{-1}$)
$FePO_4$	773	0.32	46.2	0.15	0.40
	823	0.91	39.7	0.36	0.96
	873	2.47	26.4	0.65	1.74
5 wt.% $FePO_4$/SBA-15	773	0.56	81.3	0.46	24.6
	823	1.16	72.8	0.84	45.0
	873	2.73	49.0	1.34	71.8
10 wt.% $FePO_4$/SBA-15	773	0.67	75.1	0.50	13.4
	823	1.37	63.1	0.86	23.0
	873	3.39	38.8	1.31	35.1
15 wt.% $FePO_4$/SBA-15	773	0.68	76.1	0.52	9.29
	823	1.44	61.4	0.88	15.7
	873	3.30	36.0	1.19	21.3
20 wt.% $FePO_4$/SBA-15	773	0.73	74.2	0.54	7.23
	823	1.34	61.0	0.82	11.0
	873	3.33	33.3	1.11	14.9
40 wt.% $FePO_4$/SBA-15	773	0.61	68.8	0.42	2.81
	823	1.34	50.3	0.68	4.55
	873	3.43	27.2	0.93	6.23
40 wt.% $FePO_4$/MCM-41	773	0.54	67.2	0.36	2.41
	823	1.53	42.7	0.65	4.35
	873	3.24	29.3	0.95	6.36
SBA-15	773	0.023	24.9	0.0058	–
	823	0.082	44.3	0.036	–
	873	0.23	60.2	0.14	–

Reaction conditions: $P(CH_4) = 2P(O_2) = 33.8$ kPa; catalyst, 0.20 g for supported catalysts and 0.50 g for $FePO_4$; total flow rate, 60 ml min^{-1}.

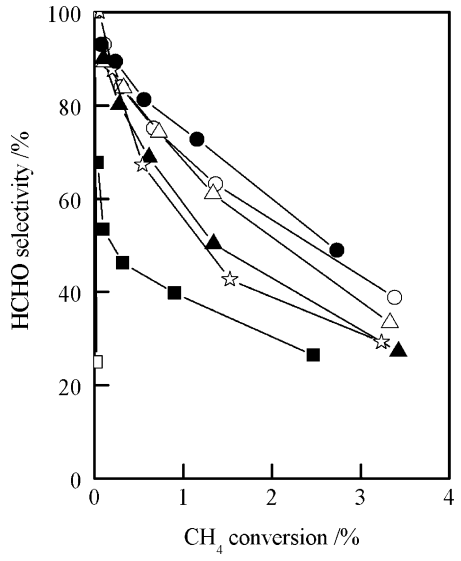

Fig. 5. HCHO selectivity vs. CH_4 conversion with O_2: (□) SBA-15, (●) 5 wt.% $FePO_4$/SBA-15, (○) 10 wt.% $FePO_4$/SBA-15, (△) 20 wt.% $FePO_4$/SBA-15, (▲) 40 wt.% $FePO_4$/SBA-15, (☆) 40 wt.% $FePO_4$/MCM-41 and (■) $FePO_4$. Conditions: $W = 0.20$ g (for supported catalysts) and 0.50 g (for $FePO_4$), $F = 60$ ml/min, $P(CH_4) = 33.8$ kPa, $P(O_2) = 16.9$ kPa, $T = 673$–873 K.

best for the selective oxidation of CH_4 to HCHO with O_2. This was different from the tendency observed for the MCM-41-supported catalyst series, where the HCHO selectivity at a given CH_4 conversion increased with the following order, $FePO_4$ ≈9 wt.% $FePO_4$/MCM-41 < 20 wt.% $FePO_4$/MCM-41 ≈40 wt.% $FePO_4$/MCM-41. As a result, the SBA-15-supported $FePO_4$ samples with lower loading amount exhibited remarkably higher HCHO selectivity than the corresponding MCM-41-supported ones.

3.3. Reaction mechanism and structure–property relationship

We carried out kinetic measurements over the SBA-15-supported $FePO_4$ samples. The results showed that the rate of CH_4 conversion was almost independent of the partial pressure of O_2 (5–70 kPa) at a fixed CH_4 partial pressure, indicating a zero order reaction with respective to O_2 in the investigated O_2 pressure range. On the other hand, at a fixed partial pressure of O_2, the rate of CH_4 conversion increased proportionally to the partial pressure of CH_4 (0–80 kPa), suggesting a first order reaction to CH_4 pressure. The same results have been obtained over the unsupported and the MCM-41-supported $FePO_4$, indicating the same reaction mechanism over these catalysts. These kinetic features suggested a redox mechanism for the conversion of CH_4 to

HCHO with O_2 as follows:

$$O_2 \rightleftarrows 2O_s$$

$$CH_4 + O_s \rightarrow CH_3(a) + OH(a)$$

$$CH_3(a) + O_s \rightarrow CH_3O(a)$$

$$CH_3O(a) + O_s \rightarrow HCHO + OH(a)$$

$$OH(a) + OH(a) \rightarrow H_2O + O_s$$

where O_s denotes the lattice oxygen in surface region. In this mechanism, CH_4 is activated by the lattice oxygen of surface, probably forming adsorbed methyl species [CH_3(a)]. HCHO is likely to be produced via the oxidation of the CH_3(a) through possibly adsorbed methoxide species [CH_3O(a)]. The kinetic results that the rate of CH_4 conversion is proportionally to the CH_4 pressure and independent of the O_2 pressure suggest that the activation of CH_4 is the rate-determining step and the replenishment of the surface oxygen by gaseous oxygen proceeds very fast.

It has been clarified that the redox property of the $FePO_4$ clusters encapsulated within the mesoporous channels of SBA-15 is enhanced. The encapsulated $FePO_4$ clusters could be reduced more easily at lower temperatures than the crystalline $FePO_4$ as shown by the TPR results in Fig. 4. The enhanced redox property of the active component would accelerate the activation of CH_4 and the formation of HCHO.

It should be noted that the encapsulation of $FePO_4$ species into MCM-41 also improves the redox property of the $FePO_4$ species. However, the SBA-15-supported catalysts exhibited remarkably higher HCHO selectivity than the MCM-41-supported samples at a given CH_4 conversion as indicated in Fig. 5. Recently, we have found that small molybdenum oxide clusters (MoO_x) encapsulated within SBA-15 are also more selective towards the partial oxidation of CH_4 to HCHO than the MoO_x within MCM-41. The larger pore diameter of the mesoporous channel of SBA-15 (ca. 5.5 nm as compared with ca. 3.0 nm of MCM-41) may be one possible reason for the high selectivity to HCHO because HCHO would desorb more easily from SBA-15. In a short communication [10], Liu et al. reported that a vanadium oxide (VO_x) supported on SBA-15 showed higher selectivity for the oxidative dehydrogenation of C_3H_8 than that supported on MCM-41. They explained that the acid sites with medium strength existing in MCM-41 might be responsible for the lower selectivity of the catalysts based on MCM-41 towards C_3H_6 while no acidity could be detected in SBA-15 with NH_3-TPD measurements. We also found that small number of acid sites was remained in MCM-41 and suggested that these acid sites were possibly the silanol groups on defective sites [14]. The absence of such acid sites in SBA-15 might indicate the difference of the nature of the framework defectiveness between MCM-41 and SBA-15. These small amount of acid sites with medium strength located in the mesoporous channels of MCM-41 would increase the probability of the consecutive conversion of the HCHO formed on the active components, and thus cause the decrease in HCHO selectivity. In other words, in addition to the larger porous diameter, the "inertness" of SBA-15 as compared with MCM-41 should be another reason for the higher selectivity of the SBA-15-supported catalysts in the partial oxidation reactions.

4. Conclusions

Small iron phosphate ($FePO_4$) clusters, in which the local coordination environment of iron was the same with that in the crystalline $FePO_4$, could be encapsulated within the mesoporous channels of SBA-15 as the loading amount of $FePO_4$ was lower than 40 wt.%. The encapsulated $FePO_4$ clusters could be reduced at remarkably lower temperatures than the crystalline $FePO_4$. Higher CH_4 conversion and HCHO selectivity were obtained over the SBA-15-supported $FePO_4$ than over the unsupported and the MCM-41-supported one. The conversion of CH_4 to HCHO was suggested to proceed via a redox mechanism and the activation of CH_4 by the surface lattice oxygen was the rate-determining step over all the $FePO_4$-based catalysts. The enhanced redox property of the encapsulated $FePO_4$ clusters within the mesoporous channels was believed to be one reason for the increased catalytic performances. The larger porous diameter and the "inertness" of SBA-15 were probably responsible for the higher HCHO selectivity of the SBA-15-supported catalysts as compared with the MCM-41-supported ones particularly with low loading amount of $FePO_4$.

Acknowledgements

This work was supported by the National Natural Science Foundation of China (Nos. 20273054 and 20021002), the Chinese Ministry of Science and Technology (No. G1999022408), the National Basic Research Program of China (grant No. 2003CB615803), the Scientific Research Foundation for the Returned Overseas Chinese Scholars, State Education Ministry and the Creative Research Foundation for Young Scientists by Fujian Province of China (No. 2001J029).

References

[1] R. Pitchai, K. Klier, Catal. Rev. Sci. Eng. 28 (1996) 13.
[2] M.J. Brown, N.D. Parkyns, Catal. Today 18 (1991) 305; N.D. Parkyns, C.I. Warburton, J.D. Wilson, Catal. Today 18 (1993) 385.
[3] T.J. Hall, J.S.J. Hargreaves, G.J. Hutchings, R.W. Joyner, S.H. Taylor, Fuel Proc. Technol. 42 (1995) 151.
[4] K. Otsuka, Y. Wang, Appl. Catal. A 222 (2001) 145.
[5] K. Tabata, Y. Teng, T. Takemoto, E. Suzuki, M.A. Banares, M.A. Pena, J.L.G. Fierro, Catal. Rev. Sci. Eng. 44 (2002) 1.

[6] Y. Wang, K. Otsuka, J. Catal. 155 (1995) 256;
Y. Wang, K. Otsuka, J. Catal. 171 (1997) 106.
[7] G.O. Alptekin, A.M. Herring, D.L. Williamson, T.R. Ohno, R.L. McCormick, J. Catal. 181 (1999) 104;
R.L. McCormick, G.O. Alptekin, D.L. Williamson, T.R. Ohno, Top. Catal. 10 (2000) 115.
[8] X. Wang, Y. Wang, Q. Tang, Q. Guo, Q. Zhang, H. Wan, J. Catal. 217 (2003) 457.
[9] D. Zhao, J. Feng, Q. Huo, N. Melosh, G.H. Fredrickson, B.F. Chmelka, G.D. Stucky, Science 279 (1998) 548.
[10] Y.-M. Liu, Y. Cao, K.-K. Zhu, S.-R. Yan, W.-L. Dai, H.-Y. He, K.-N. Fan, Chem. Commun. (2002) 2832.
[11] H.H. Lopez, A. Martinez, Catal. Lett. 83 (2002) 37.
[12] B. Lin, X. Wang, Q. Guo, W. Yang, Q. Zhang, Y. Wang, Chem. Lett. 32 (2003) 860.
[13] W. Yang, X. Wang, Q. Guo, Q. Zhang, Y. Wang, New J. Chem. 27 (2003) 1301.
[14] Q. Zhang, Y. Wang, Y. Ohishi, T. Shishido, K. Takehira, J. Catal. 202 (2001) 308.